FeCo nanoparticles as antibacterial agents with improved response in magnetic field: an insight into the associated toxicity mechanism

To cite this article: Moditma *et al* 2021 *Nanotechnology* **32** 335101

IOP Publishing Nanotechnology
Nanotechnology 32 (2021) 335101 (14pp) https://doi.org/10.1088/1361-6528/abfa53

FeCo nanoparticles as antibacterial agents with improved response in magnetic field: an insight into the associated toxicity mechanism

Moditma[1], Priyanka Singh[2], Raksha Sharma[3], Anita K Verma[2] and S Annapoorni[1]

[1] Department of Physics and Astrophysics, University of Delhi, Delhi—110007, India
[2] Nano-biotech Laboratory, Zoology Department, Kirori Mal College, University of Delhi, Delhi—110007, India
[3] Physics Department, Kirori Mal College, University of Delhi, Delhi—110007, India

E-mail: annapoornis.phys@gmail.com

Received 25 December 2020, revised 2 April 2021
Accepted for publication 21 April 2021
Published 25 May 2021

Abstract

The emergence of multi-drug resistant bacterial infections has resulted in increased interest in the development of alternative systems which can sensitize bacteria to overcome resistance. In an attempt to contribute to the existing literature of potential antibacterial agents, we present here, a first report of the antibacterial potential of FeCo nanoparticles, both as stand-alone devices and in presence of magnetic field, against the bacterial strains of *S. aureus* and *E. coli*. A relatively simple polyol process was employed for nanoparticle synthesis. Formation of FeCo alloy in the desired BCC phase was confirmed by x-ray diffraction with a high saturation magnetization ($M_s \sim 180$ Am^2kg^{-1}). Uniformly sized spherical structures with sharp edges were obtained. Solution stability was confirmed by the zeta potential value of -27.8 mV. Dose dependent bacterial growth inhibition was observed, the corresponding linear correlation coefficients being, $R^2 = 0.74$ for *S. aureus* and $R^2 = 0.76$ for *E. coli*. Minimum inhibitory concentration was accordingly ascertained to be >1024 μg ml^{-1} for both. Bacterial growth curves have been examined upon concomitant application of external magnetic field of varying intensities and revealed considerable enhancement in the antibacterial response upto 64% in a field of 100 mT. An effort has been made to understand the bacterial inhibitory mechanism by relating with the chemical and physical properties of the nanoparticles. The ease of field assisted targeting and retrieval of these highly magnetic, antibacterial nano-devices, with considerably improved response with magnetic fields, make them promising for several medical and environment remediation technologies.

Supplementary material for this article is available online

Keywords: FeCo nanoparticles, antibacterial, reactive oxygen species (ROS), minimum inhibitory concentration (MIC), toxicity mechanism, magnetic field

(Some figures may appear in colour only in the online journal)

1. Introduction

Antibacterial drugs have long been used to treat several infectious diseases. However, the increased use of such 'wonder' drugs has resulted in the emergence of multidrug-resistant pathogenic strains of bacteria, which pose serious health concerns across the globe [1]. Several drug-resistant strains of bacteria have been identified, like those of *Staphylococcus aureus*, which is resistant to the commonly used drugs like penicillin, sulfonamide, methicillin and vancomycin; macrolide-resistant *Streptococcus pyogenes*; vancomycin-resistant *Enterococcus* and the bacteria *Neisseria gonorrhoeae* (PPNG), *Salmonella enterica*, *Escherichia coli*, *Klebsiella pneumonia*; all of which are resistant to the drug penicillin [2]. According to an estimate of the Infectious Diseases Society of America, over 70% of the nosocomial infections in the United States are caused by multidrug-resistant bacterial strains [3]. The appearance of such pathogenic strains can increase clinical complications in terms of higher drug doses, treatments involving higher toxicity, longer hospital stays and hence greater societal expenses, leading to uncontrolled epidemics in a worst possible scenario [4–6]. Therefore, alternative treatment options should be formulated, which are effective in deactivating the disease-causing bacteria, without any possibility for the development of resistances in these strains.

The emergence of nanotechnology has allowed for such alternatives, by devising novel materials and strategies to combat bacterial resistance. This includes the use of nanoparticles that exhibit antibacterial potential [7]. Additionally, employing external stimulants like electric and magnetic fields have been identified as potentially appealing techniques for bacterial growth inhibition [8, 9]. These can serve as non-contact methods for bacterial decontamination. The advantage of using such alternative techniques is the simultaneous application of multiple mechanisms that can cause bacterial damage. This would make it difficult for simultaneous mutations to occur in the same bacterial cell, which is required in order to develop resistance [2]. Nanoparticle engineering can be done to load one or more antibacterial agents in a single device [4, 10], which would again restrict development of resistance by the collective set of damaging mechanisms. Another advantage offered by nanoparticles is the possibility to achieve targeted delivery of the antibiotic at the infected site, which results in increased local dosage with less amount of antibiotic, and also fewer harmful effects to the healthy cells [2, 4]. Also, the high surface area to volume ratio of the nanoparticles allows for more reactive sites for the bacteria-nanoparticle interaction, thus causing more detrimental effects [11, 12].

Antibacterial properties of the nanoparticles could also be useful in food packaging and as coatings on medical implants and devices for making them resistant to several bacterial infections [13]. Additionally, usability of these antibacterial agents in water purification has been proposed by several groups [14–16], which could help to lower the operational costs of conventional water treatment technologies [16]. Zero valent iron (ZVI) nanoparticles are of particular interest in this regard, where besides the antimicrobial action, reductive decomposition of the organic pollutants to less toxic forms, aids water decontamination [17, 18]. Markova *et al* for example proposed the use of bimetallic Fe-Ag nanoparticles, to serve the dual purpose of microbial decontamination (by Fe and Ag) and phosphate removal (by Fe) in water bodies [10]. Here, the use of magnetic core of iron allows the possibility of efficient targeting and safe removal of the nano-disinfectants from the site of action by using external magnets. Similar magnetically active biocidal nano-structures have been proposed for various antibacterial applications, where the magnetic component aids localized action and post-treatment removal [19–21]. The possibility of re-usability of the retrieved biocides has also been explored, with considerable success upto 3–5 cycles, for cases such as silver coated iron oxide nanoparticles, by Mosaiab *et al* [22] and Theamdee *et al* [23]. Another advantage offered by magnetic anti-bacterials is their ability to penetrate through bacterial biofilms causing cell disruption deep within the biofilms on application of external magnetic fields [6, 24, 25]. Conventional anti-bacterials like Ag, though highly efficient against planktonic bacteria are ineffective in eradicating bacterial biofilms due to poor penetration through the films [6]. Hence, antibacterial loading onto magnetic nanoparticles becomes important to increase efficacy against bacterial biofilms.

Among various ferromagnetic materials, FeCo alloy has the highest saturation magnetization of 2.45 T [26]. The high magnetization has encouraged the use of these alloy nanoparticles in various biomedical applications, such as MRI, magnetic hyperthermia and targeted drug delivery [27, 28], where iron oxide nanoparticles (IONPs) are conventionally used. Thus, with the aim of further extending their possible use in the medical field, the present work has been undertaken to explore the antibacterial potential of FeCo nanoparticles, individually and in conjugation with an external magnetic field. The antibacterial response can also be exploited for usage in various other applications such as water disinfection, food packaging and textile industry. The advantage offered by magnetic FeCo nanoparticles over conventionally proposed antibiotic nanostructures could be envisaged by their ability to serve as single-entity magnetic antibacterials, without the need for extensive engineering of core–shell nanostructures to achieve easy targetability and retrieval. This would save the unnecessary investment of time, cost and complexity in the synthesis procedures. Bacterial inactivation by ZVI nanoparticles has been extensively studied by several groups [11, 29, 30]. The main mechanisms of toxicity being identified as the highly reactive nature of iron in water, resulting in reductive decomposition of biomolecules, along with the oxidative stress imposed by ROS produced from Fenton's chemistry. Cobalt based nanomaterials have also recently gained interest in the biomedical field. This includes the improved antibacterial response due to contact killing mode, as in the case of cobalt-doped titania heterostructures[31] and also as Co_3O_4 nanoparticles exhibiting enzymatic SOD and catalase like behavior for excess ROS management [32]. It would be interesting to look at the antibacterial potential of the alloyed species exhibiting higher magnetization, in

addition to an increase in the possible toxicity mechanisms due to the two contributory species involved. Additionally, the antibacterial behavior in presence of an external magnetic field, with a possible synergistic response as indicated by previous studies [33, 34], if found to be the case, would be of great clinical and technological relevance.

In this report, the antibacterial effects of FeCo alloy nanoparticles have been assessed on *E. coli* and *S. aureus* as model organisms for Gram negative and Gram positive bacteria, respectively. The motivation for choosing these species was their widespread environmental presence besides being an important class of drug-resistant bacteria, responsible for causing several infectious diseases in humans [35]. This is an attempt to understand the antibacterial response of highly magnetic FeCo alloy nanoparticles individually and in three magnetic field intensities, namely 13 mT, 35 mT and 100 mT. Dose dependent growth inhibition has been evaluated in terms of minimum inhibitory concentration (MIC). Comparison in terms of growth curves of bacterial cultures with/without magnetic fields along with the possible toxicity mechanisms by correlating with the nanoparticle properties have been presented.

2. Materials and methods

2.1. Materials

For the synthesis of FeCo nanoparticles, the salts ferrous sulfate heptahydrate ($FeSO_4.7H_2O$, 99.0% pure) and cobalt acetate tetrahydrate ($Co(OAc)_2.4H_2O$, 98% pure) were purchased from Sigma Aldrich. Sodium hydroxide (NaOH) pellets and the solvent ethylene glycol (analytical grade) were supplied by SRL Pvt. Ltd., India. All the chemicals were used as such without further purification.

For antibacterial tests, bacterial strains of *E. coli* (MTCC-1677) and *S. aureus* (MTCC-3160) were procured from the Institute of Microbial Technology (IMTECH), Chandigarh, India. Nutrient broth, nutrient agar and gentamycin were purchased from Hi-Media Laboratories Pvt. Ltd. (Mumbai, India). DCFH-DA was purchased from Sigma Aldrich, USA. Deionized water was used throughout the experiment.

2.2. Synthesis of nanoparticles

FeCo nanoparticles were synthesized by using ethylene glycol as the reducing agent. The procedure was adopted from an earlier report [36] and involves addition of equal concentrations of $FeSO_4.7H_2O$ and $Co(OAc)_2.4H_2O$ to ethylene glycol heated near its boiling temperature at 180 °C. NaOH pellets were also added after salt addition to promote the rate of forward reaction. The reaction mixture achieved greyish color, indicating alloy formation and was subsequently removed from the hot plate. The unreacted/impurity salts were washed off using ethanol and water. The washed nanoparticles were left at room temperature for vacuum drying.

2.3. Nanoparticle Characterization

The synthesized nanoparticles were characterized for their structural properties using x-ray diffractometer (XRD, Rigaku Ultima IV), operated at 20 kV, 20 mA with Cu-Kα x-rays ($\lambda = 1.5405$ Å) in the 2θ range of 40° to 120°. Magnetic properties were assessed by obtaining the M–H curves in a vibrating sample magnetometer (VSM, Micro-Sense EV9). Information for nanoparticle size and surface charge was obtained using Zetasizer Nano ZS, Malvern Panalytical, which operates on the principle of dynamic light scattering (DLS). For morphological characterizations, Field emission scanning electron microscope (FESEM, ZEISS Gemini SEM 500) operated at 10 kV and Transmission electron microscope (TEM, JEOL 2100F) operated at 200 kV were used. Energy dispersive x-ray spectrometer (EDS, Octane Elect Super SDD) attached to the FE-SEM, stand-alone Energy dispersive x-ray fluorescence spectrometer (ED-XRF, Fischer) and Inductively coupled plasma atomic emission spectrometer (ICP-AES, SPECTRO Analytical instruments, ACROS) were used for elemental analysis. Surface studies of the nanoparticles were performed by x-ray photoelectron spectroscopy (XPS, Physical Electronics, PHI 5000 VersaProbe III).

2.4. Magnetic field set-up

Static magnetic fields (SMF) of 13 mT, 35 mT and 100 mT were generated as per the setup depicted in figure 1. It consisted of 2 ferrite magnets, procured locally, separated by spacer materials of varying heights, to generate uniform field at the center, as measured with the help of a Digital Gaussmeter (DGM—102, SES Instruments). The control flask with standard bacterial inoculum and the experimental flask containing test samples of FeCo nanoparticles were appropriately placed at the experimental site. The entire setup was sealed in a plastic box and placed in shaker incubator for growth kinetic studies.

2.5. Antibacterial assays

2.5.1. Preparation of bacterial culture media. Nutrient broth was prepared as per manufacturer's instruction and autoclaved at 120 °C, 15 psi pressure for 20 min. Mother inoculum in 1:100 ratios was used for inoculating the sterile broth. This was left for overnight incubation in an orbital shaker incubator at 37 °C. Medium turbidity after 24 h indicated culture growth. Optical absorbance at 600 nm was measured by UV spectrophotometer (Cary 60 UV–Vis, Agilent Technologies) and colony forming unit/ml (CFU ml^{-1}) was determined as: $1OD = 0.8 \times 10^9$ CFU ml^{-1}.

2.5.2. Determination of zone of inhibition (ZOI). Antibacterial susceptibility of nanoparticles was estimated by Kirby Bauer method. Culture suspension with soft agar was poured on to the nutrient agar plate. Paper disks of 5 mm each were loaded with 10 μl of test samples of FeCo nanoparticles, Gentamycin (positive control) and Milli-Q water (negative control) and

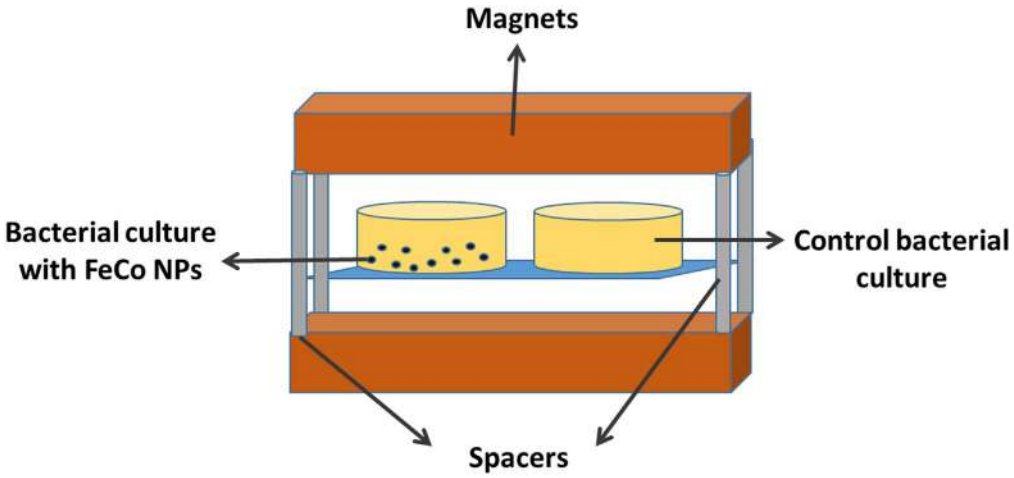

Figure 1. Schematic setup for magnetic field response.

were placed in the plate with previously divided section. The plates were placed in incubator overnight at 37 °C and ZOI was measured the next day.

2.5.3. Determination of minimum inhibitory concentration (MIC). Various nanoparticle concentrations of 32 μg ml^{-1}, 64 μg ml^{-1}, 128 μg ml^{-1}, 256 μg ml^{-1} and 1024 μg ml^{-1} were prepared and added to the bacterial culture media, as microdilutions in the 96 well plate. Absorbance value for each was measured at 600 nm after 24 h and MIC values estimated using the protocol adopted by Dey *et al* [37].

2.5.4. Growth kinetics. Sterile broth inoculated with bacterial culture was taken. Appropriate amount of the test sample of FeCo nanoparticles was added to the experimental flask, while the control flask contained normal bacterial culture. The effect of test sample on bacterial growth kinetics curve with/without the influence of applied magnetic field was recorded. Absorbance values at 600 nm were measured as a function of time, for experimental and control flasks, to obtain the growth curves.

2.5.5. Determination of reactive oxygen species (ROS). ROS generation from FeCo nanoparticles was measured using 2′,7′-dichlorofluorescein diacetate (DCFH-DA) that is a widely accepted technique for directly measuring the redox state of the cell. DCFH-DA which is cell permeable, and a non-fluorescent precursor of DCF is used as an intracellular probe for oxidative stress. It is extremely sensitive to changes in the redox state of a cell, economical, easy to use and a good indicator to follow changes in ROS over time. Intracellular ROS, post treatment with nanoparticles was estimated by previously published protocol [38]. Briefly, 1×10^9 CFU ml^{-1} were initially treated with 500 μg ml^{-1} nanoparticles for 24 h along with respective controls. The cells were thereafter pelleted by centrifugation at 5000 rpm for 2–5 min, washed 3 times with PBS pH-7.4 and later incubated for 30–40 min with DCFH-DA dye (25 μM) at 37 °C in a shaker. Pelleted cells were re-suspended in PBS and the fluorescence intensity at 528 nm wavelength was measured using an excitation source of 485 nm in a Spectro-fluorimeter (Agilent Technology, U.S.A). The percentage ROS generated was plotted against the experimental as well as the control groups.

2.6. Sample preparation for SEM imaging

To understand the effect of nanoparticles on bacterial morphology, preparation of bacterial samples were done according to the protocol by Singh *et al* [39]. Briefly, 1×10^5 CFU ml^{-1} of bacterial culture was initially treated with FeCo nanoparticles for 4 h along with the respective control groups. After that, the cells were centrifuged at 5000 rpm for 2–5 min, washed 3 times with PBS pH-7.4, followed by fixation of cells with 2.5% glutaraldehyde for 2–4 h. The cells were again washed 3 times with PBS and then dehydrated using alcohol in gradients (10%, 20%, 30%, 50%, 70%, 90%), each for 10 min and the final dehydration was done in 100% alcohol. The dehydrated cells were then re-suspended in PBS and finally mounted on to the coverslips for imaging in a Scanning Electron Microscope (SEM, ZEISS, Evo 18).

2.7. Statistical analysis

The ROS results were depicted as mean ± standard deviation. Comparison among groups were analyzed by the one-way analysis of variance (ANOVA) and means were separated by Tukey's test using Prism (8.0) software (Prism software Inc. CA). Level of significance were accepted at $p \leqslant 0.05$ level.

3. Results

3.1. Material Properties

3.1.1. Structural. X-ray diffraction pattern of the synthesized FeCo nanoparticles is shown in figure 2(a). The observed peaks at the various 2θ values correspond to (110), (200), (211), (220) and (310) planes of the BCC crystal structure of FeCo alloy, as per JCPDS card number 00-044-1433. Lattice constant was determined to be (2.856 Å), corresponding to the equiatomic alloy composition. The crystallite size

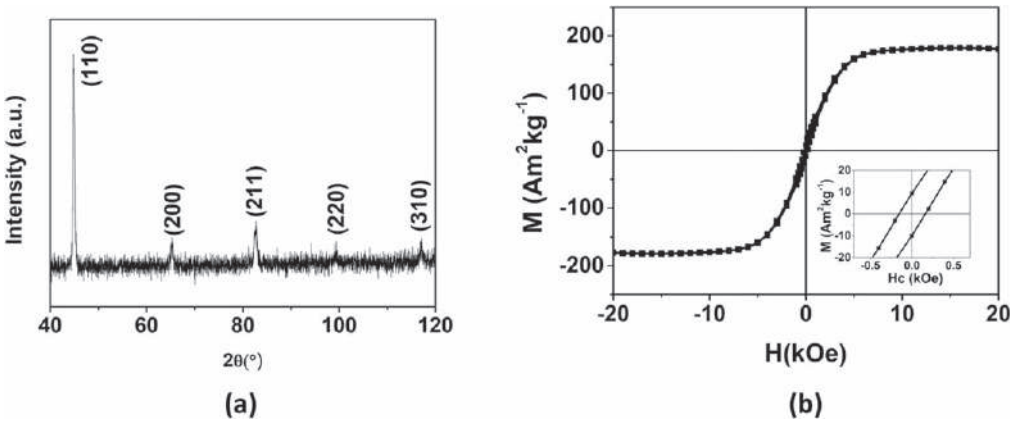

Figure 2. (a) X-ray Diffraction pattern and (b) M–H curve of FeCo nanoparticles.

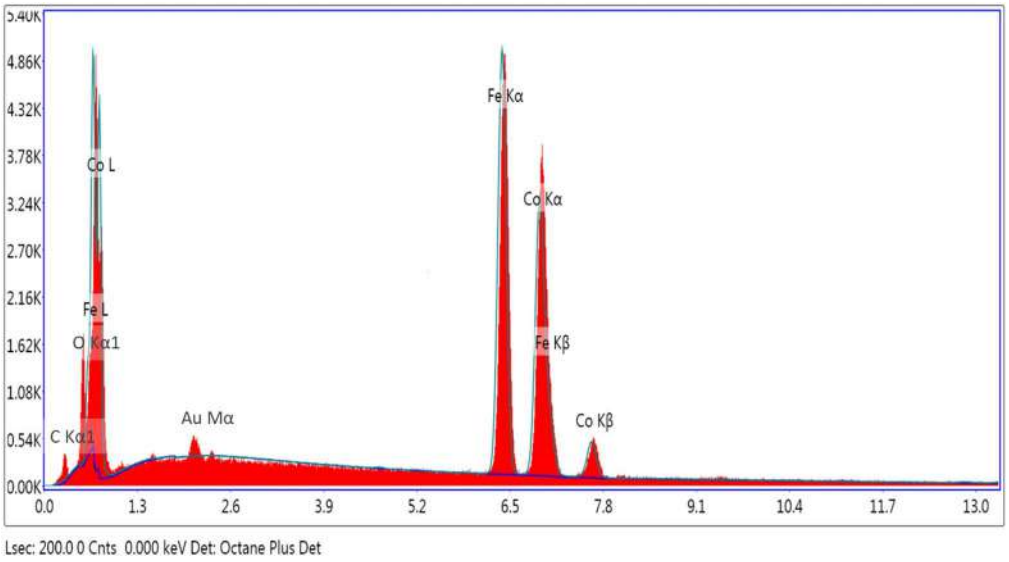

Figure 3. SEM-EDX pattern FeCo nanoparticles.

estimated from Debye–Scherrer's formula was found to be 18 nm. All peaks correspond to the BCC phase of FeCo alloy, without any additional impurity phases to be detected from the XRD pattern.

3.1.2. Magnetic. Bulk magnetic behavior was studied by obtaining the room temperature hysteresis curve using a VSM and has been depicted in figure 2(b). The samples were clearly highly magnetic, with the prepared alloy possessing a saturation magnetization (M_s) of ~180 Am^2kg^{-1}. This is large enough to allow efficient targeting and removal of the antibacterial nanoparticles using a simple hand magnet. Also, the prepared nanoparticles were stable when stored in ambient conditions upto a test period of 6 months, as depicted in our earlier report [36]. Thus the high magnetization, along with the air stability make the nanoparticles of great use as efficient magnetic antibacterial agents.

3.1.3. Composition. Energy dispersive x-ray spectroscopy (EDX), energy dispersive x-ray fluorescence (XRF) and inductively coupled plasma atomic emission spectroscopy (ICP-AES) were used to determine the composition of alloy. The EDX pattern (figure 3) revealed the nanoparticles to be dominantly composed of Fe and Co elements, amounting to 55% and 45%, respectively. This was further ascertained with ICP-AES analysis which confirmed the alloy composition to be $Fe_{53}Co_{47}$. The stand-alone bench-top EDXRF elemental analyzer also revealed the alloy composition to be $Fe_{51}Co_{49}$ (Figure S1 available online at stacks.iop.org/NANO/32/335101/mmedia). The estimated alloy composition thus corroborates well within experimental error limits and confirms the formation of equiatomic alloy composition.

3.1.4. Morphological. To characterize the nanoparticles for their morphology, electron microscopy images were obtained. Formation of monodispersed spherical nanostructures was apparent from the FE-SEM image (figure 4(a)). This was confirmed by the lognormal fit of nanoparticle size distribution stating an average particle diameter of 219 ± 17 nm, as reported previously [36]. To get a deeper

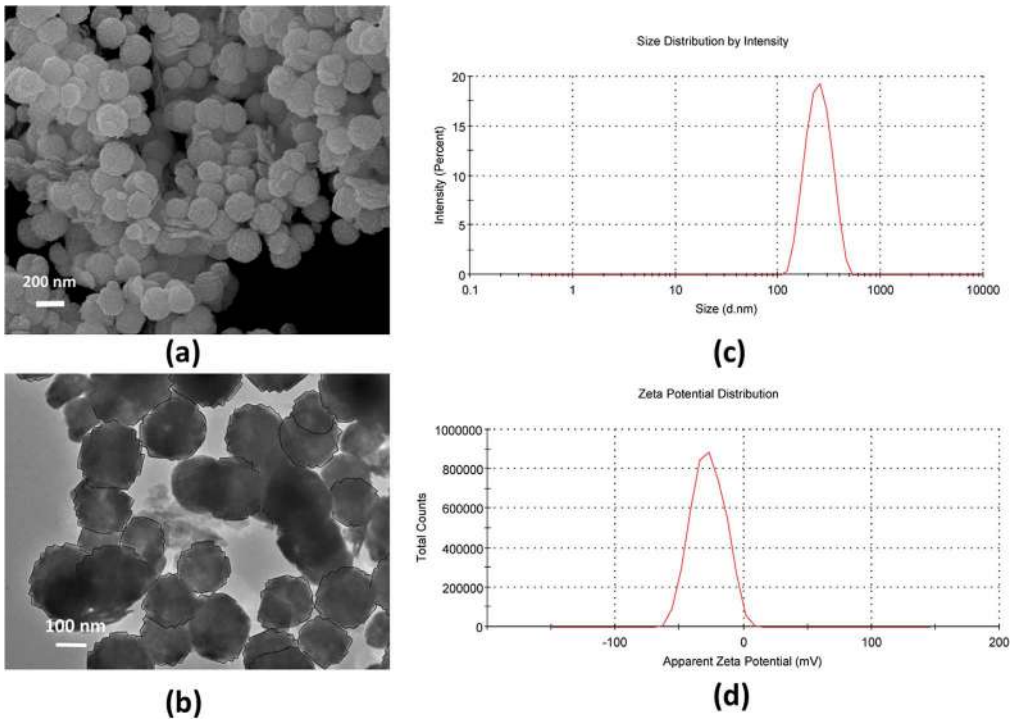

Figure 4. (a) FE-SEM and (b) TEM image of the nanoparticles. (c) Size distribution obtained from DLS. (d) Zeta potential of the nanoparticles.

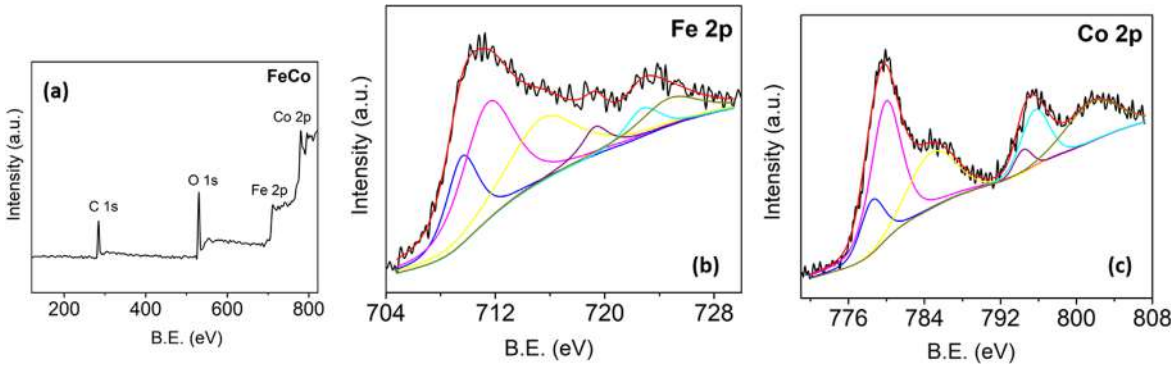

Figure 5. (a) XPS survey scan and high resolution XPS spectra of (b) Fe 2p and (c) Co 2p of FeCo nanoparticles.

insight into the particle morphology, bright field TEM images were recorded, as shown in figure 4(b). The nanostructures evidently have sharp cubical edges making up the nanospheres, which has been highlighted in the image.

3.1.5. Particle size and zeta potential. The mean hydrodynamic diameter determined from DLS measurements was found to be 285 nm, with a polydispersity index (PDI) of 0.299, as shown in figure 4(c). The small PDI indicates homogeneity and narrowness of the particle size distribution, thus corroborating the uniform size distribution obtained from FE-SEM images. Zeta potential as shown in figure 4(d) was determined to be −27.8 mV and indicated good colloidal stability of the nanoparticles in the medium [40].

3.1.6. Surface chemistry. The chemical composition of the nanoparticle surface was determined using XPS studies. The wide scan XPS spectrum (figure 5(a)) reveals presence of C, O, Fe and Co elements [41]. Presence of carbon is attributed to carbon contamination during sample preparation, in addition to the organic synthesis process adopted. Surface oxidation of the nanoparticles leads to the occurrence of oxygen peak. High resolution XPS spectra of Fe 2p and Co 2p peaks were recorded to understand the respective valence states and have been depicted in figures 5(b) and (c). For Fe 2p, the peaks at 709.6 and 722.8 eV are attributed

Table 1. Bacterial inhibition using FeCo nanoparticles.

Sample	Zone of inhibition - ZOI (mm)	
	E. coli	*S. aureus*
Positive control (Gentamycin: 5 mg ml^{-1})	10	8
Negative control	0	0
FeCo (10 mg ml^{-1})	0.5	0.5

to Fe (II) oxidation sates of Fe $2p_{3/2}$ and Fe $2p_{1/2}$ respectively. Peaks at 711.5 eV and 724.7 eV correspond to Fe (III) oxidation state [42]. Additional satellite peaks also appear at 715.4 eV and 719.2 eV due to Fe(II) and Fe(III), respectively. For Co 2p, the peaks at 778.5 eV and 794.3 eV are ascribed to $2p_{3/2}$ and $2p_{1/2}$ states of metallic cobalt. Peaks at 779.9 eV and 795.6 eV, with the corresponding satellite peaks at 784.8 eV and 801.7 eV occur due to presence of Co (II) oxidation state [43, 44]. The high resolution spectra clearly indicate that iron is mostly present in an oxidized state, whereas cobalt does exist in the metallic state, with slight oxidation. This might be attributed to the larger resistance against oxidation of cobalt as compared to iron, as also noted in previous studies [45].

3.2. Antibacterial activities

3.2.1. Zone of inhibition. Antibacterial potential of FeCo alloy nanoparticles against the bacterial strains of *E. coli* and *S. aureus* were investigated by performing disc diffusion assay on solid agar plates using the Kirby-Bauer method [46]. The results have been summarized in table 1, with the corresponding plate images shown in figure 6. At the nanoparticle concentration of 10 mg ml^{-1}, ZOI was determined to be 0.5 mm for both the bacterial species, suggesting nearly similar susceptibility of both to the synthesized nanoparticles.

3.2.2. Minimum inhibitory concentration. To quantify the antibacterial properties, standard broth dilution were performed and percentage growth inhibition of the bacterial strains was determined, at different nanoparticle doses, i.e. 32 μg ml^{-1}, 64 μg ml^{-1}, 128 μg ml^{-1}, 256 μg ml^{-1}, 1024 μg ml^{-1}. A positive linear correlation was observed between the nanoparticle concentration and percentage growth inhibition, which was estimated from the decreased turbidity of the culture medium. The square of the linear correlation coefficient (R^2) was correspondingly determined as 0.74 for *S. aureus* (figure 6(c)) and 0.76 for *E. coli* (figure 6(d)), clearly attributing the observed toxic effect on bacterial cultures in the presence of nanoparticles in the culture medium. The MIC values were accordingly established to be greater than 1024 μg ml^{-1} for both *S. aureus* and *E. coli.*

3.2.3. Growth curves. Growth kinetic studies were done with/without simultaneous application of external magnetic fields of varying intensities, to explore the inhibitory effect of nanoparticles on bacterial cultures. Figure 7 clearly shows a deviation from the normal culture growth. Treatment with FeCo nanoparticles resulted in an inhibition of 18% in the growth of *S. aureus* after 24 h of incubation (figure 7(a)). This was greatly enhanced by successive application of higher magnetic fields, reaching a net inhibition of 64% with a simultaneous application of a field of 100 mT. In case of *E. coli*, an inhibition of 20% was observed with FeCo nanoparticles, which increased to 63% upon simultaneous application of 100 mT magnetic field, as shown in figure 7(b). Figures 7(c) and (d) represent the effect of individual magnetic fields on bacterial growth. An increasing antibacterial trend with application of higher magnetic fields was observed, the maximum being ~ 30% for a field of 100 mT in *S. aurues* and 27% in *E. coli.* It can thus be inferred that simultaneous application of magnetic fields significantly enhances the antibacterial potential of the synthesized FeCo nanoparticles. This can be attributed to the additive effect of the two bactericidal pathways, also considering the enhanced local magnetic flux density due to the highly magnetic FeCo nanoparticles.

3.2.4. ROS Generation. DCFH-DA is a popular fluoresence-based probe for ROS detection *in vitro*. Figure 8 represents the percentage of ROS produced as a result of nanoparticle treatment (500 μg ml^{-1}). It was observed that the generated ROS levels in *S. aurues* were comparatively higher than *E. coli*, being 128% in FeCo treated cultures which increased to 230% for simultaneous application of 100 mT magnetic field. In case of *E. coli*, an increase of 108% was observed for FeCo nanoparticles as compared to control and increased upto 208% upon field application.

3.2.5. SEM Photomicrographs: To visualize the bactericidal effect due to nanoparticle treatment, SEM photomicrographs were recorded. Figure 9(a) shows the spherical shape of *S. aurues*, with an approximate diameter of 1 μm, while *E. coli* cells exhibited their characteristic rod-like morphology, being ~1 μm in length, as depicted in figure 9(b). The cell walls of the untreated bacteria were smooth without indentations. Interaction with FeCo nanoparticles caused significant cell damage. As seen in figure 9(c) in *S. aureus* treated with FeCo nanoparticles, significant rupture of cell wall and distortions in morphology was evident, and has been highlighted in the inset. Debris surrounding the bacterial cells suggested subsequent leakage of cytoplasmic contents. Similar damage to *E. coli* cells and the associated deformations in shape was evident from figure 9(d). Here the cytoplasm oozing out of the bacterial cell was clearly discernible and has been marked with an arrow, thus

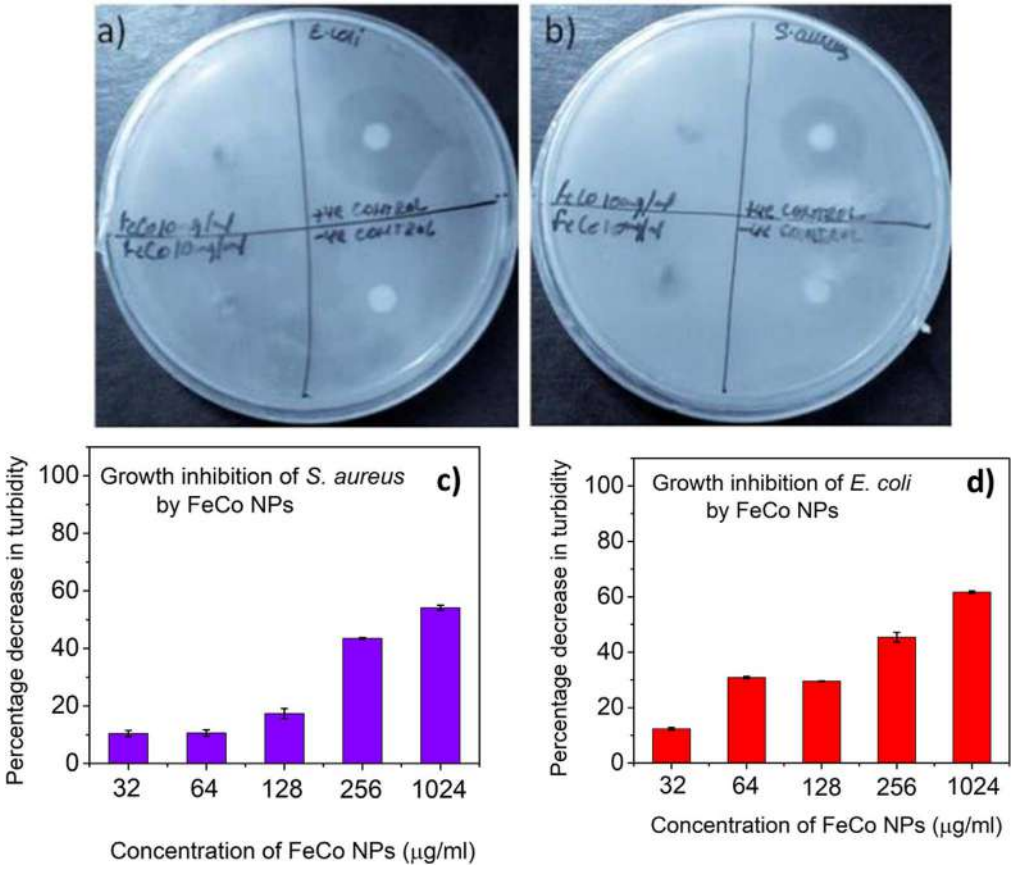

Figure 6. Zone of inhibition of (a) *E. coli* and (b) *S. aureus* using FeCo nanoparticles. Dose dependent growth inhibition of (c) *S. aureus* and (d) *E. coli*. Note: Data is represented as mean ± standard deviation of two identical experiments.

indicating complete loss of cell integrity. Thus, SEM images clearly indicated a significant cellular damage upon interaction with nanoparticles.

4. Discussions

The synthesized FeCo nanoparticles were highly magnetic with a uniform size distribution and exhibited notable antibacterial potential, with increased efficacy on exposure to magnetic field. The underlying reasons for the observed antibacterial response could be attributed to the interplay of several probable factors working in orchestration which result in inflicting damage to bacterial cells.

The esterases in the cytosol cleave the DCFH-DA at the two ester bonds producing a comparatively polar and membrane-impermeable non-fluorescent molecule-H2DCF that accumulates in the cytosol and its oxidation then yields DCF which is a highly fluorescent product. The redox state of the sample can then be monitored over time by detecting the increase in the fluorescence. The results confirmed generation of free radicals from the surface oxidation of FeCo, which becomes toxic to bacterial cells leading to death. ROS include oxygen-derivatives such as superoxide anion ($O_2^{\bullet -}$), hydrogen peroxide (H_2O_2) and hydroxyl free radical ($OH^{\bullet}$), which are naturally produced as a by-product of various aerobic metabolic pathways and in low/moderate concentrations serve as second messengers for various cellular responses. Excess ROS generation may attack the membrane lipids causing a breakdown of the membrane function. Certain transition metals might disrupt the cellular donor ligands that coordinate Fe causing oxidative damage to the cellular constituents such as DNA, lipids and proteins, which in turn leads to several deleterious effects such as alteration of membrane fluidity, protein cross linking, mutations in DNA sequence, inactivation of respiratory enzymes, among others, ultimately leading to cell death [47].

Figure 10 schematically illustrates the possible toxicity induced by FeCo alloy nanoparticles. These nanoparticles in the extracellular space can (1) either be confined to the extracellular environment, or enter the cells *via* endocytosis (2) or passive diffusion (3). Partial dissolution may occur in both spaces, extracellular as well as endocellular, with the release of ions of iron and cobalt (4), that may also enter the cells *via* specific metalloproteins receptors or by non-specific receptors. Once internalized, both FeCo nanoparticles and ions dispense in the cytoplasm. Both ions and the nanoparticles induce oxidative stress by increasing ROS production, leading to formation of intramolecular disulfide motifs (A), lipid and protein peroxidation, with cell membrane disruption (B and C), and DNA damage apoptosis (D).

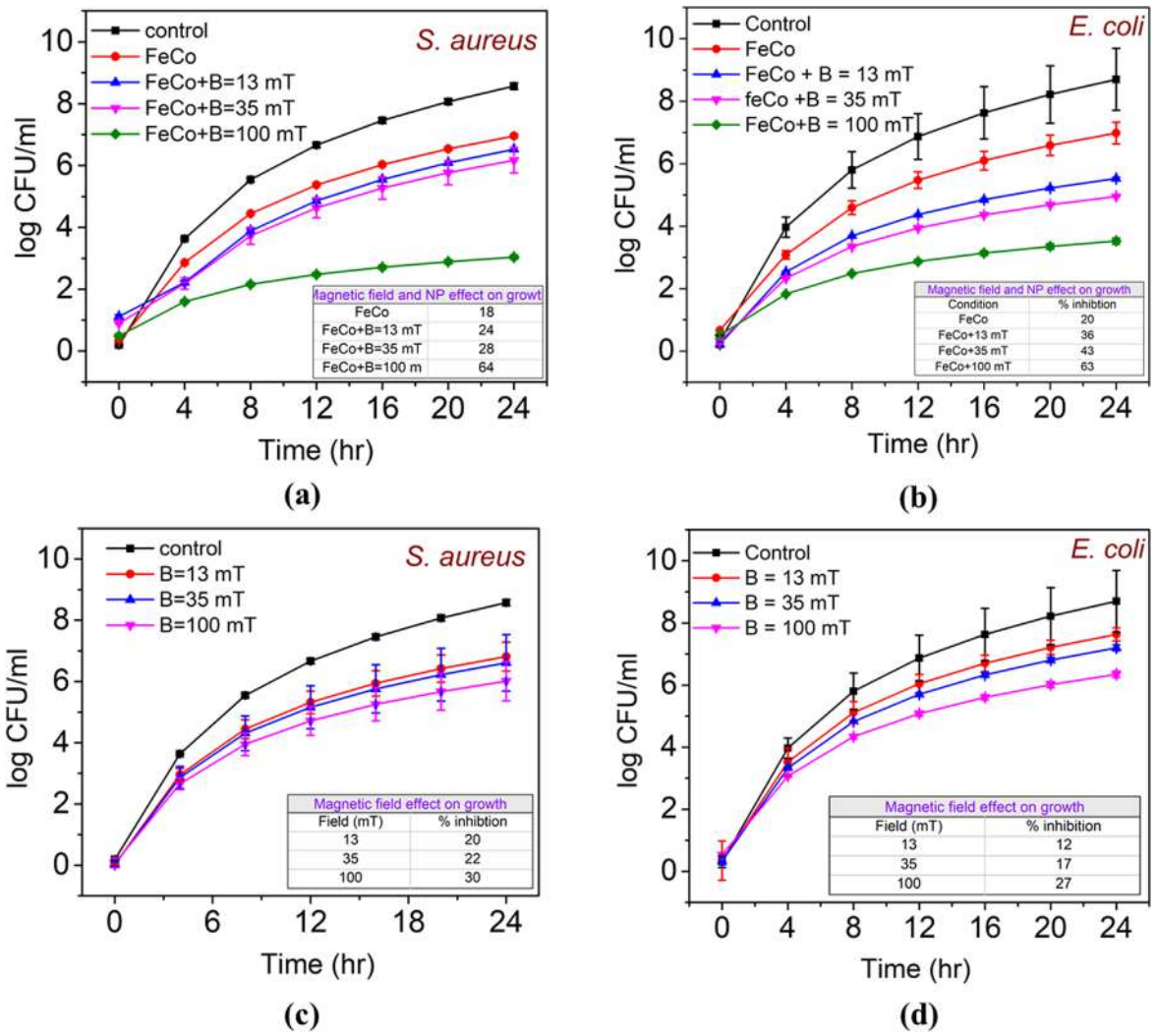

Figure 7. Growth curves of (a), (c) *S. aureus* and (b), (d) *E. coli* in presence of FeCo nanoparticles and/or magnetic field. Values are represented as mean ± standard deviation of two identical experiments.

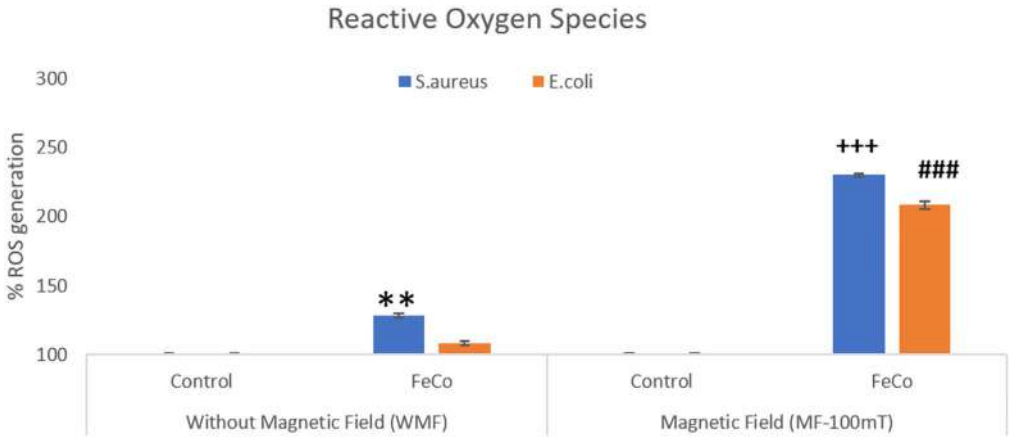

Figure 8. Percentage ROS generation in FeCo nanoparticles treated bacterial strains *S. aureus* and *E. coli* with or without magnetic field. Data were expressed in mean ± Standard deviation ($N = 2$). * denote significant difference between control versus FeCo NPs treated group WMF in *S. aureus* + denote significant difference between control versus FeCo NPs treated group in presence of MF in *S. aureus* # denote significant difference between control versus FeCo NPs treated group in presence of MF in *E. coli* $^{*}p<0.05$; $^{**}p<0.01$; $^{***}p<0.001$.

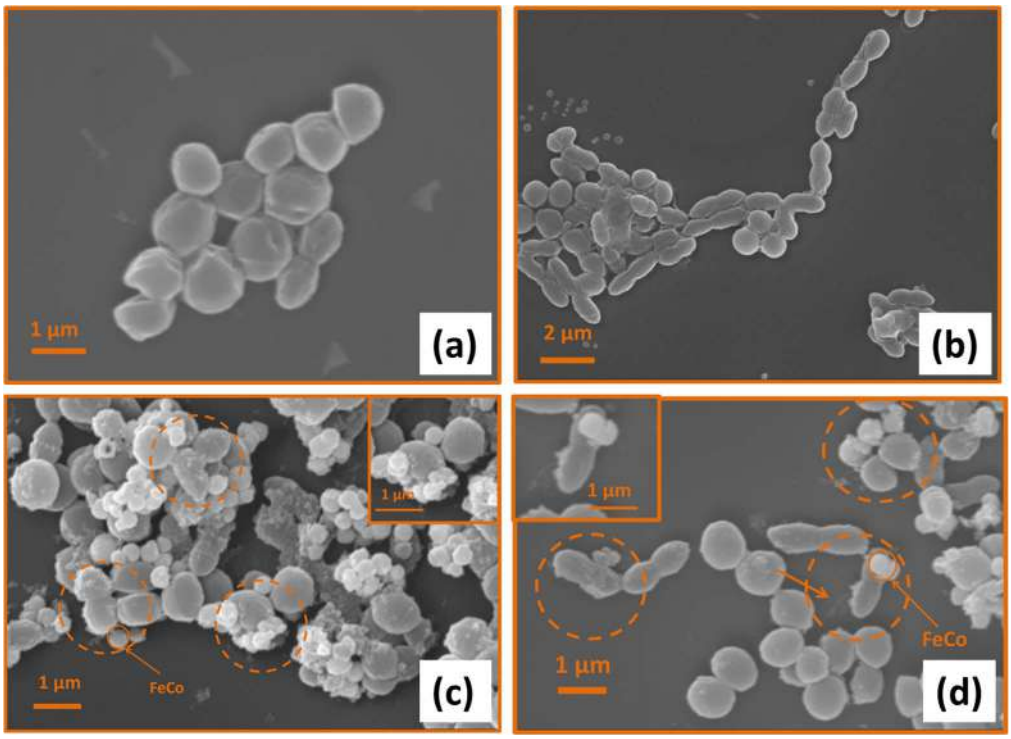

Figure 9. (a) SEM photomicrographs of untreated (a) *S. aureus* and (b) *E. coli* cells. SEM image of FeCo nanoparticles treated (c) *S. aureus* and (d) *E. coli* cells. Inset highlights the damage caused to the bacterial cells.

Figure 11 represents the possible mechanistic pathways triggered by FeCo alloy nanoparticles leading to enhanced ROS generation, along with other possible toxicity routes that have been stated as follows:

FeCo alloy nanoparticles when dispersed in the aqueous bacterial cultures, are susceptible to surface oxidation from the dissolved oxygen, a case well reported for metallic iron [11, 29, 48]. The possible oxidation processes can be understood by comparing the oxidation-reduction potentials of the various half reactions involved and have been depicted in figure 11(A). For metallic iron, the reaction,

$$Fe^{+2} + 2e^{-} \rightleftharpoons Fe^{0},$$

is characterized by a standard reduction potential of −0.44 V [49]. The corresponding reduction potential for cobalt is, E^{0} $[Co^{+2}/Co^{0}] = -0.28$ V [49]. This is lower than the standard reduction potential (E^{0}) of various biological redox active couples, which lie in the range from −0.38 V to +0.34 V [50]. Hence, reductive decomposition of various biomolecules, like the functional groups in membrane proteins, would be facilitated by spontaneous electron exchanges occurring at the nanoparticle-bacterial interface. Alternatively, the electrons might be taken up by free oxygen to give superoxide free radicals, where the reduction potential, E^{0} $[O_2\,(aq)/O_2^{\bullet -}] = -0.16$ V [51] is more than that of iron and cobalt. Fe^{0} and Co^{0} may further facilitate reduction of molecular oxygen by the 2-electron (E^{0} $[O_2\,(g), H^{+}/H_2O_2] = 0.69$ V) and 4-electron (E^{0} $[O_2\,(g), H^{+}/H_2O\,(liq)] = 1.23$ V) processes, the latter being more energetically favorable clearly. However, since only 2 electrons are involved, H_2O_2 production is significant during oxygen reduction by many species [52]. For example, in the case of metallic iron, the initial oxidation of Fe^{0} under aerobic conditions has been reported via the 2-electron process [53–55],

$$Fe^{0} + O_2 + 2H^{+} \rightarrow Fe^{+2} + H_2O_2.$$

Though the more dominant mechanism of oxygen mediated corrosion of iron is given by the 4-electron process, viz.,

$$2Fe^{0} + O_2 + 2H_2O \rightarrow 2Fe^{+2} + 4OH^{-}.$$

the 2-electron process can cause considerable H_2O_2 production in the medium [53, 55]. Thus produced high levels of ROS at the nano-bio interface can compromise cell integrity by lipid peroxidation or protein modifications. The resulting disorganization and deformity in membrane structure effects membrane permeability, thus adversely effecting ion transport and cellular respiratory functions, besides making leakage of essential cytoplasmic components probable. Additionally, the ability of H_2O_2 to readily cross bacterial membranes allows its action far from site of production [56, 57]. Thus it permeates through the cell wall and can cause oxidative damage to intracellular components as well, such as the Fe-S clusters, where it may readily take up Fe^{+2} to form more dangerous hydroxyl free radicals ($OH^{\bullet}$), via the Fenton reaction [58]:

$$Fe^{+2} + H_2O_2 \rightarrow Fe^{+3} + OH^{-} + OH^{\circ}$$

The produced Fe^{+3} ions can be further reduced to Fe^{+2} ions by the superoxide free radicals, owing to a larger value of the reduction potential of the iron redox couple

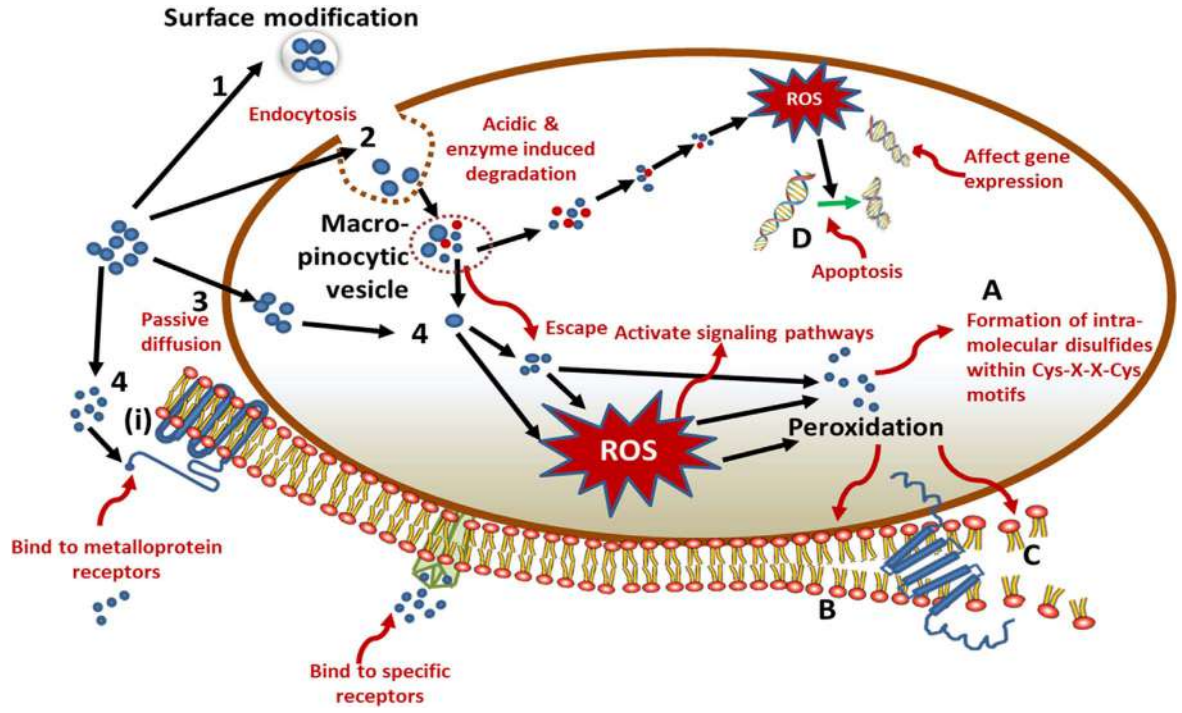

Figure 10. Bactericidal pathway of FeCo nanoparticles damage to bacterial cell.

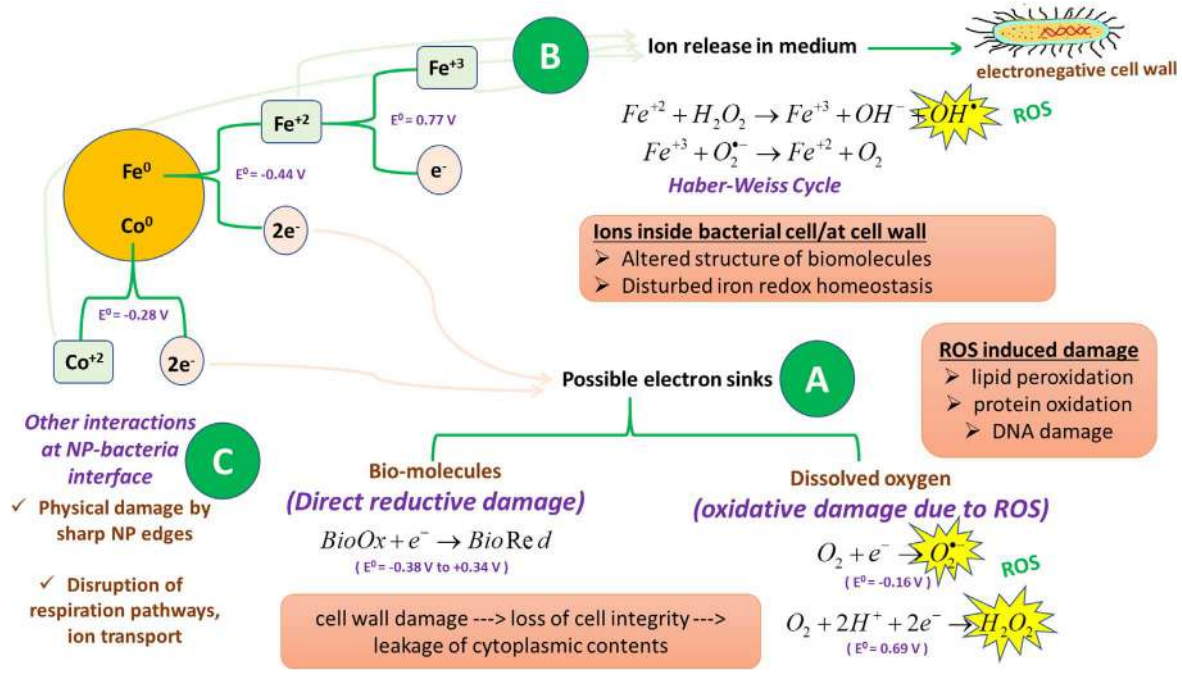

Figure 11. Toxicity scheme of FeCo alloy to bacterial cultures: (A) Electron exchange mediated damage (B) Ion-induced damage (C) Damage due to NP-bacteria interfacial interaction.

(E^0 [Fe^{+3}/Fe^{+2}] = 0.77 V) [49]:

$$Fe^{+3} + O_2^{\circ-} \rightarrow Fe^{+2} + O_2.$$

This continuous redox cycling of the ionic species, called as the Haber−Weiss cycle has been depicted in figure 11(B) and results in production of large amounts of hydroxyl ions in the medium, which can cause severe oxidative damages.

There also exists a possibility of release of the ionized species into bacterial suspension, as noted in earlier studies [11, 29, 59]. The resulting toxicity pathways have been shown in figure 11(B). Electrostatic interactions between the electronegative cell wall [12] and the positive ions may cause these ions to travel to the cell wall and into the cytoplasm [11, 12], where they can form coordination complexes with

the cellular ligands, thus altering structure and function of various biomolecules as suggested previously [60]. Interactions with membrane-associated molecules may result in membrane depolarization and deformation, again endangering cell integrity. Further, the presence of Fe^{+2} ions in the medium would promote excess ROS production by the Haber −Weiss cycle described above and would significantly disturb the cellular iron homeostasis.

Another instance highlighted in scheme of figure 11(C) suggests a possibility of the nanoparticles' adherence at bacterial cell wall, as has been observed from the TEM images of various studies [29, 61]. Nanoparticle interaction with the cell surface is a source of chemical or physical toxicity to the cell. The sharp edges of the adhering nanoparticles, as noted from electron microscopy images, might be responsible for physically disrupting the cell envelope as in [62, 63]. The damaged cell wall could further allow leakage of various cellular components (figure 10). Also their strong adsorption on cell wall may disrupt the ion transport chains and cellular respiratory mechanisms.

For the case of magnetic field induced bacterial inhibition, several investigations have been reported in literature to decipher the effect/response of magnetic field upon living systems. Various theories have been put forth for the same. One is the free radical theory which suggests formation of oxygen free radicals such as O^{2-}, $OH^{\bullet}$, $HO_2^{\bullet}$ in the bacterial suspension upon exposure to magnetic fields [64, 65]. As noted above, excessive presence of such ROS is responsible for causing oxidative stress in bacteria. Another argument usually stated is Rosen's membrane theory [66, 67], which suggests rotation of the membrane phospholipids in presence of external magnetic fields. Molecular reorientations within the membrane would lead to functional disruption of the embedded ion channels, thus effecting ion mobility. Yet another theory is the ion interference mechanism given by Binhi *et al* [68, 69], where magnetic fields have been suggested to affect the probability of dissociation of the ion-protein complexes. The observed sequential inhibition in bacterial growth upon magnetic field exposures of increasing intensities could be attributed to such structural and functional changes in the bacterial cell.

To justify the proposed mechanism, the role of electron-exchange mediated bacterial damage has been assessed by comparing the antibacterial potentials of iron and cobalt nanoparticles synthesized by similar chemical routes with that of FeCo alloy nanoparticles, in an applied magnetic field of 100 mT. The corresponding growth curves have been attached as a separate supplementary data in figures S2 (a)–(d). It was observed that Co nanoparticles exhibit significantly higher bacterial inhibition when compared to Fe nanoparticles for both the bacterial species. This might be related to the higher tendency for surface oxidation of synthesized Fe nanoparticles as compared to Co nanoparticles, as noted in XPS measurements above for the case of FeCo nanoparticles (figure 5(a)) and also in previous studies [45]. As noted (from the half reactions mentioned) above, this would allow further scope for oxidation of Co nanoparticles in the bacterial culture than Fe and hence more electron exchanges, thus resulting in more ROS generation and direct damage to cellular components. The results are thus in agreement with previous studies suggesting that chemically stable species have negligible cytotoxic effects while the ones with a potential to get oxidized or reduced are more toxic to cellular organisms [29, 50, 70]. The redox contributions from Fe and Co might thus clearly be assigned to be a possible toxicity route of the synthesized FeCo nanoparticles.

The associated increase in levels of ROS in the medium has been depicted in figure S3. The corresponding values have been presented in table S1. Clearly nanoparticle treatment results in generation of higher levels of ROS as compared to the control. The excessive ROS prodcution in Co nanoparticles treated bacteria can be associated to the higher oxidation tendencies of Co nanoparticles as discussed above. Also significant increase in ROS levels was observed for the case of magnetic field treated samples, in accordance with the free radical theory described above.

Thus from the above work, we can conclude that FeCo nanoparticles with external magnetic fields exhibits additive antibacterial activity, with the added advantage of magnet-assisted targeting and removal from the site of action. As a next step, studies can be performed to see if similar (or maybe better) response maybe triggered even for small exposure times, as noted by Ji *et al* [71].

5. Conclusions

FeCo nanoparticles have been successfully synthesized by polyol reduction and characterized for their structural, magnetic, morphological and antibacterial properties. The synthesis process results in the formation of highly magnetic, uniformly sized spherical nanoparticles with sharp edges, as observed from the TEM images. Antibacterial studies reveal a positive linear correlation between nanoparticle dosage and percent growth inhibition of *S. aureus* and *E. coli*. The MIC values of FeCo nanoparticles were correspondingly determined to be greater than 1024 μg ml^{-1} for both the species. Antibacterial efficacy of nanoparticles increased significantly in presence of external magnetic fields, as observed from the bacterial growth curves, with a maximum growth inhibition in external magnetic field of 100 mT. Based on the observed antibacterial response, possible proposed bacterial toxicity routes were ROS induced reductive damage of biomolecules, metal-ion induced damage, along with the physical damage by the sharp-edged nanostructures. The synthesized FeCo nanoparticles thus serve as potential candidates for self-sufficient magnetic antibacterial systems for localized action, with the improved performance upon magnetic field stimulation. Being technologically very relevant for areas such as magnet assisted therapies and small exposure times which would help to cut down the cost and energy involved in bacterial decontamination processes.

Acknowledgments

The authors M. and P.S. acknowledge CSIR, India and UGC, India respectively for assistance in form of fellowship. Central Experimentation Facility (CEF) of the Department of Physics and Astrophysics, University of Delhi and University Science Instrumentation Center (USIC), University of Delhi is acknowledged for the experimental facilities. We are also grateful to the Advanced Instrumentation Research Facility (AIRF) of Jawaharlal Nehru University, Delhi for the TEM measurements. Institute Instrumentation Center (IIC), IIT Roorkee and Sophisticated Analytical Instrument Facility (SAIF), IIT Bombay are respectively acknowledged for XPS and ICP-AES measurements. We thank Sophisticated Analytical Instrument Facility (SAIF), AIIMS for SEM viewing of the bacterial cells. We are also grateful to SERB-DST for the SERB project EMR/2016/002437 for financial support.

Data availability statement

The data generated and/or analyzed during the current study are not publicly available for legal/ethical reasons but are available from the corresponding author on reasonable request.

ORCID iDs

S Annapoorni https://orcid.org/0000-0002-6083-300X

References

[1] Davies J and Davies D 2010 *Microbiol. Mol. Biol. Rev.* **74** 417–33
[2] Pelgrift R Y and Friedman A J 2013 *Adv. Drug Deliv. Rev.* **65** 1803–15
[3] Clatworthy A E, Pierson E and Hung D T 2007 *Nat. Chem. Biol.* **3** 541–8
[4] Huh A J and Kwon Y J 2011 *J. Control. Release* **156** 128–45
[5] Riley M A, Robinson S M, Roy C M, Dennis M, Liu V and Dorit R L 2012 *Biochem. Soc. Trans.* **40** 1438–42
[6] Mahmoudi M and Serpooshan V 2012 *ACS Nano* **6** 2656–64
[7] Hajipour M J, Fromm K M, Akbar Ashkarran A, Jimenez de Aberasturi D, de Larramendi I R, Rojo T, Serpooshan V, Parak W J and Mahmoudi M 2012 *Trends Biotechnol.* **30** 499–511
[8] Singh A and Dubey A K 2018 *ACS Appl. Bio. Mater.* **1** 3–20
[9] Brkovic S, Postic S and Ilic D 2015 *Appl. Oral Sci.* **23** 179–86
[10] Marková Z, Šišková K M H, Filip J, Čuda J, Kolář M, Šafářová K, Medřík I and Zbořil R 2013 *Environ. Sci. Technol.* **47** 5285–93
[11] Lee C, Jee Y K, Won I L, Nelson K L, Yoon J and Sedlak D L 2008 *Environ. Sci. Technol.* **42** 4927–33
[12] Stoimenov P K, Klinger R L, Marchin G L and Klabunde K J 2002 *Langmuir* **18** 6679–86
[13] Bhushan A K, Kumar M, Periyasamy Y and Viswanath L 2018 *Appl. Nanosci.* **8** 137–53
[14] Chou W L, Yu D G and Yang M C 2005 *Polym. Adv. Technol.* **16** 600–7
[15] Wang T, Ma B, Jin A, Li X, Zhang X, Wang W and Cai Y 2018 *J. Hazard. Mater.* **342** 392–400
[16] Ramalingam B, Khan M M R, Mondal B, Mandal A B and Das S K 2015 *ACS Sustainable Chem. Eng.* **3** 2291–302
[17] Lowry K M and Johnson G V 2004 *Environ. Sci. Technol.* **38** 5208–16
[18] Matheson L J and Tratnyek P G 1994 *Environ. Sci. Technol.* **28** 2045–53
[19] Wang L, Luo J, Shan S, Crew E, Yin J, Zhong C J, Wallek B and Wong S S S 2011 *Anal. Chem.* **83** 8688–95
[20] Hoop M, Shen Y, Chen X Z, Mushtaq F, Iuliano L M, Sakar M S, Petruska A, Loessner M J, Nelson B J and Pané S 2016 *Adv. Funct. Mater.* **26** 1063–9
[21] Shatan A B, Venclíková K, Zasońska B A, Patsula V, Pop-Georgievski O, Petrovský E and Horák D 2019 *Pharm. Res.* **36** 147–58
[22] Mosaiab T, Jeong C J, Shin G J, Choi K H, Lee S K, Lee I, In I and Park S Y 2013 *Mater. Sci. Eng. C* **33** 3786–94
[23] Theamdee P, Rutnakornpituk B, Wichai U, Nakkuntod M and Rutnakornpituk M 2015 *J. Ind. Eng. Chem.* **29** 63–70
[24] Wang X, Wu J, Li P, Wang L, Zhou J, Zhang G, Li X, Hu B and Xing X 2018 *ACS Appl. Mater. Interfaces* **10** 34905–15
[25] Subbiahdoss G, Sharifi S, Grijpma D W, Laurent S, Van Der Mei H C, Mahmoudi M and Busscher H J 2012 *Acta Biomater.* **8** 2047–55
[26] Sourmail T 2005 *Prog. Mater. Sci.* **50** 816–80
[27] Seo H *et al Nat. Mater.* 2006 **5** 971–6
[28] Kline T L, Xu Y H, Jing Y and Wang J P 2009 *J. Magn. Magn. Mater.* **321** 1525–8
[29] Auffan M, Achouak W, Rose J, Roncato M A, Chanéac C, Waite D T, Masion A, Woicik J C, Wiesner M R and Bottero J Y 2008 *Environ. Sci. Technol.* **42** 6730–5
[30] Diao M and Yao M 2009 *Water Res.* **43** 5243–51
[31] Li J, Wang J, Wang D, Guo G, Yeung K W K, Zhang X and Liu X 2017 *ACS Appl. Mater. Interfaces* **9** 27475–90
[32] Dong J, Song L, Yin J J, He W, Wu Y, Gu N and Zhang Y 2014 *ACS Appl. Mater. Interfaces* **6** 1959–70
[33] Bae J E *et al Biomaterials* 2011 **32** 9401–14
[34] Bajpai I, Balani K and Basu B 2014 *J. Biomed. Mater. Res.* B **102** 524–32
[35] Méndez-Pfeiffer P A, Soto Urzúa L, Sánchez-Mora E, González A L, Romo-Herrera J M, Gervacio Arciniega J J and Martínez Morales L. J. 2019 *J. Appl. Phys.* **125** 213102
[36] Moditma S, Choudhary S, Vashisht G, Reddy V R and Annapoorni 2019 *J. Supercond. Nov. Magn.* **33** 1653–7
[37] Dey A, Dasgupta A, Kumar V, Tyagi A and Verma A K 2015 *Int. Nano Lett.* **5** 223–30
[38] Tyagi A, Rawat K, Verma A K and Bohidar H B 2016 *Anal. Methods* **8** 1060–8
[39] Singh I, Priyam A, Jha D, Dhawan G, Gautam H K and Kumar P 2020 *Mater. Sci. Eng. C* **107** 110284
[40] Chandrasekar N, Kumar K M M, Balasubramnian K S, Karunamurthy K and Varadharajan R 2013 *Dig. J. Nanomater. Bios.* **8** 765–75
[41] Jaffari G H, Lin H, Rumaiz A K, Yassitepe E, Ni C and Shah S I 2013 *Phys. Status Solidi Appl. Mater. Sci.* **210** 306–10
[42] Yamashita T and Hayes P 2008 *Appl. Surf. Sci.* **254** 2441–9
[43] Gao X, Tan S C, Wee A T S, Wu J, Kong L, Yu X and Moser H O 2006 *J. Electron Spectros. Relat. Phenomena* **150** 11–4
[44] Bazylewski P, Boukhvalov D W, Kukharenko A I, Kurmaev E Z, Hunt A, Moewes A, Lee Y H, Cholakh S O and Chang G S 2015 *RSC Adv.* **5** 75600–6

[45] Kumar H, Ghosh S, Srivastava P, Kabiraj D, Avasthi D K, Olivi L and Aquilanti G 2013 *Adv. Mater. Lett.* **4** 390–7
[46] Bauer A W, Kirby W M, Sherris J C and Turck M 1966 *Am. J. Clin. Pathol.* **36** 493–6
[47] Dharmaraja A T 2017 *J. Med. Chem.* **60** 3221–40
[48] Davenport A J, Oblonsky L J, Ryan M P and Toney M F 2000 *J. Electrochem. Soc.* **147** 2162
[49] Bratsch S G 1989 *J. Phys. Chem. Ref. Data* **18** 1–21
[50] Auffan M, Rose J, Wiesner M R and Bottero J Y 2009 *Environ. Pollut.* **157** 1127–33
[51] Wood P M 1987 *Trends Biochem. Sci* **12** 250–1
[52] Wood P M 1988 *Biochem. J* **253** 287–9
[53] Joo S H, Feitz A J, Sedlak D L and Waite T D 2005 *Environ. Sci. Technol.* **39** 1263–8
[54] Zečević S, Dražić D M and Gojković S 1989 *J. Electroanal. Chem.* **265** 179–93
[55] Le Bozec N, Compère C, L'Her M, Laouenan A, Costa D and Marcus P 2001 *Corros. Sci.* **43** 765–86
[56] Sirelkhatim A, Mahmud S, Seeni A, Kaus N H M, Ann L C, Bakhori S K M, Hasan H and Mohamad D 2015 *Nano-Micro Lett.* **7** 219–42
[57] Sharma P, Jha A B, Dubey R S and Pessarakli M 2012 *J. Bot.* **2012** 1–26
[58] Touati D 2000 *Arch. Biochem. Biophys.* **373** 1–6
[59] Song W, Zhang J, Guo J, Zhang J, Ding F, Li L and Sun Z 2010 *Toxicol. Lett.* **199** 389–97
[60] Saleh N B, Chambers B, Aich N, Plazas-Tuttle J, Phung-Ngoc H N and Kirisits M J 2015 *Front. Microbiol.* **6** 1–8
[61] Morones J R, Elechiguerra J L, Camacho A, Holt K, Kouri J B, Ramírez J T and Yacaman M J 2005 *Nanotechnology* **16** 2346–53
[62] Argueta-Figueroa L, Torres-Gómez N, García-Contreras R, Vilchis-Nestor A R, Martínez-Alvarez O, Acosta-Torres L S and Arenas-Arrocena M C 2018 *Prog. Nat. Sci. Mater. Int.* **28** 447–55
[63] Okyay T O, Bala R K, Nguyen H N, Atalay R, Bayam Y and Rodrigues D F 2015 *RSC Adv.* **5** 2568–75
[64] Kohno M, Yamazaki M, Kimura I and Wada M 2000 *Pathophysiology* **7** 143–8
[65] Strašák L, Vetterl V and Šmarda J 2002 *Bioelectrochemistry* **55** 161–4
[66] Rosen A D 1993 *Biochim. Biophys. Acta (BBA)—Biomembranes* **1148** 317–20
[67] Rosen A D 1996 *Biochim. Biophys. Acta (BBA)—Biomembranes* **1282** 149–55
[68] Binhi V N, Alipov Y D and Belyaev I Y 2001 *Bioelectromagnetics* **22** 79–86
[69] Binhi V N 1997 *Electr. Magnetobiol.* **16** 203–14
[70] Thill A, Zeyons O, Spalla O, Chauvat F, Rose J, Auffan M and Flank A M 2006 *Environ. Sci. Technol.* **40** 6151–6
[71] Ji W, Huang H, Deng A and Pan C 2009 *Micron* **40** 894–8